# *Active Materials for Innovative Organic Solar Cells and Smart Heterogeneous Catalysts Based on Porous Aromatic Frameworks*

**Ph.D. THESIS in Organic chemistry**
**Doctoral school of Faculty of Chemistry and Chemical Engineering,**
**Cluj-Napoca**
**Public defense July, 7th 2022**
**Cluj-Napoca**
**by Natalia Terenti**

**Jury:**

| | | |
|---|---|---|
| *President:* | *Acad. Cristian Silvestru* | *Babeş-Bolyai University, Cluj-Napoca, Romania* |
| *Scientific advisor:* | *Prof. Dr. Ion Grosu* | *Babeş-Bolyai University, Cluj-Napoca, Romania* |
| *Reviewers:* | *Conf. Dr. Niculina-Daniela Hădade* | *Babeş-Bolyai University, Cluj-Napoca, Romania* |
| | *Prof. Dr. Vasile. I. Pârvulescu* | *University of Bucharest, Romania* |
| | *Conf. Dr. Augustin Mădălan* | *University of Bucharest, Romania* |

**SUMMARY**

*Keywords: organic solar cells, acceptors, donors, single materials, porous aromatic frameworks, heterogeneous catalysis*

## *General introduction*

The thesis, structured in two distinct parts, presents the contributions brought in the field of organic solar cells (OSCs) and heterogeneous catalysis.

The first part contains a detailed study of the optoelectronic and photovoltaic properties of a series of new acceptor-donor-acceptor (A-D-A) and donor-acceptor (D-A) systems.

Three isomers of indacenodithiophene were synthesized in order to investigate the influence of the mode of linkage of the thienyl unities to the phenyl central unit on the optoelectronic properties. Their properties were investigated by cyclic voltammetry, fluorescence and UV-Vis spectroscopy.

Next, we decided to synthesize a series of molecules based on **IDT-1** structure by modification of the end-capping units. A comparative study of new symmetric and nonsymmetric compounds shows the potential use of these derivatives as *p*- and *n*-type semiconductor materials for bulk heterojunction organic solar cells (BHJ OSCs).

The next chapter includes a systematic analysis of chemical structure – properties – power conversion efficiency relationship in a series of new small D-A molecules based on triarylamine donor block connected to indanedione-based acceptors by thienyl and phenyl conjugated bridges. The compounds were tested in Single Molecular Organic Solar Cells (SMOSCs) in both direct and inverted structures

The second part of the thesis focuses on the synthesis, characterization and investigation of the catalytic properties of two porous materials based on a linear linker and tetrahedral units. The new Porous Aromatic Frameworks (PAFs) (namely *PAF-1* and *PAF-2*) entrapped within their structure copper (I), palladium (II) and palladium (0) species were used as heterogeneous catalysts in palladium catalyzed cross-coupling reactions and in copper-catalyzed reactions.

## 1. General considerations

A solar cell or a photovoltaic cell (PC), is an electrical device used to transform sunlight in electricity through the photovoltaic effect. There are two main categories of solar cells, depending on material used for fabrication: inorganic and organic. Despite all advantages that organic solar cells present, in particular their low cost and fabrication methods, important technological development is still required for their large-scale applications.

## 2. Original contributions

### 2.1. Indacenodithiophene (IDT) core for new acceptors and donors

### 2.1.1. Acceptors based on isomers of indacenodithiophene unit

A fundamental research work was done order to investigate the influence of the thiophene rings fusion mode to the central benzene unit on the optical and electronic properties of the molecule: changing from the usual indaceno[*1,2-b:5,6-b'*]dithiophene (IDT-1) to indaceno[*2,1-b:6,5-b'*]dithiophene (IDT-2) and indaceno[*1,2-c:5,6-c'*]dithiophene (IDT-3).

### 2.1.1.1. Synthesis of compounds

The target compounds are fused-ring systems containing as donor the IDT unit (D) with tetrahexylphenyl as side chain groups and dicyanovinyl as terminal acceptor units (A) (figure 1).[1]
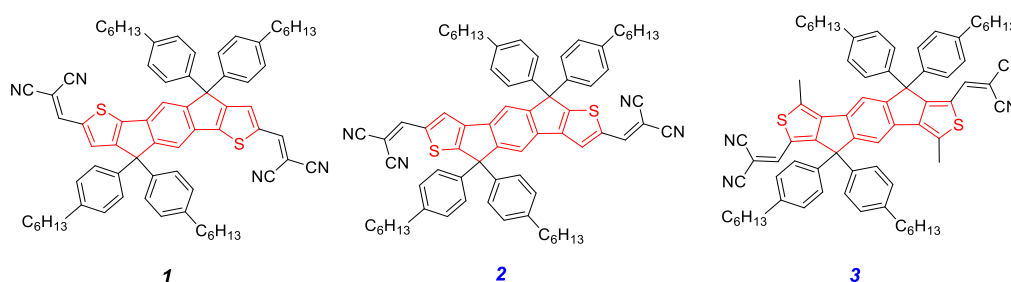


**Figure 1.** The chemical structures of target compounds *1*, *2* and *3*

The synthesis of compounds *1–3* is depicted in scheme 1. The first intermediates 2,5-bis(2'-thiophenyl) diethylterephthalate were obtained by a Stille cross-coupling reaction (in the case of compound *6*) or by a Suzuki-Miyaura cross-coupling reactions (in the case of compounds *12* and *15*). Treatment of 1-bromo-4-hexylbenzene (*7*) with butyllithium at $-78^{\circ}$C gave a lithio-compound which was then reacted with corresponding dithienyl-terephalate derivative to give, after a double acid-promoted intramolecular cyclization reaction sequence, the IDT intermediates *7*, *13* and *16*. Dialdehyde intermediate *9* and *14* were accessed *via* a Vilsmeier reaction, using POCl₃ and anhydrous DMF in dry 1,2-dichloroethane, while dialdehyde intermediate *17* was obtained by Rieche formylation. The target compounds were obtained by a Knoevenagel reaction of their corresponding dialdehyde (*9*, *14* and *17*) with malononitrile *10*.

---

[1] N. Terenti, A. P. Crisan, S. Jungsuttiwong, N. D. Hădade, A. Pop, I. Grosu and J. Roncali, *Dyes Pigm.*, 2021, **187**, 109116;

### 2.1.1.2. Solid-state investigations

Single crystals of compounds *9*, *14* and *2* were obtained by slow evaporation of petroleum ether/dichloromethane mixture and analyzed by X-Ray diffraction. Compound *9* and *14* crystallize in the centrosymmetric monoclinic (*P-1*) space group, with two molecules in the asymmentric unit, while compound *2* crystalizes in the centrosymmetric triclinic *P-1* space group, with only one molecule present in the asymmentric unit cell. The IDT part of derivatives *9* and *14* is fully planar and both formyl units exhibit *S-cis* configurations (figure 2). No contacts between the fused aromatic units are observed for compound *9*.

In the case of compound *14*, the crystallographic structure reveals intermolecular interactions between H atoms from a hexyl group and the indacenodithiophene core of a neighboring molecule (H··· π, d = 2.753 Å,) resulting in a supramolecular chain.
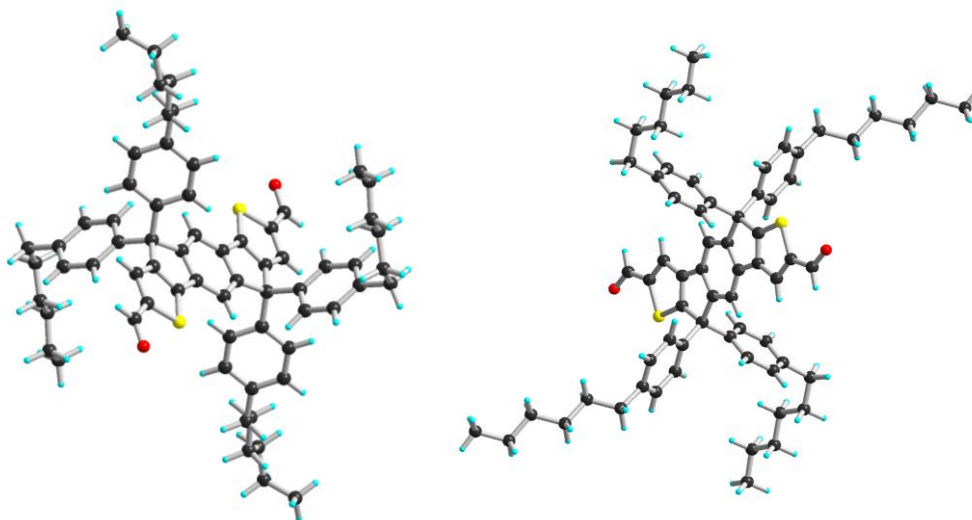


**Figure 2**. X-Ray single crystal structure of compound *9* (left) and 14 (right)

In the case of compound *2*, the IDT-DCV conjugated system is also completely planar with both DCV acceptor units in S-cis configuration. In the crystal lattice each molecule interacts with two neighbors arranged on both sides of the IDT core. The IDT units are arranged parallel to each other at a distance of 3.389 Å in a head-to-tail manner.

### 2.1.1.3. Optical and electrochemical properties

The absorption properties of the target compounds *1*, *2* and *3*, respectively, and of their corresponding intermediates were investigated by UV-Vis absorption spectroscopy. The UV-Vis absorption spectra were recorded both in methylene chloride solutions and as thin films spun-cast on glass and the corresponding data are collected in table 1. In the absorption spectra of the target compounds the first transition in the 300–400 nm region could be ascribed to the π-π* transition of the indacenodithiophene moiety while the absorption bands in the 400–600 nm region for compound *1*, 400–500 for compound *2* and 400–450 nm for compound *3* (figure 3) could be assigned to the internal charge transfer (ICT) between the electron-rich indacenoditiophene (IDT) core and the dicyanovinylene (DCV) groups.[2]

---

[2] S. Roquet, A. Cravino, P. Leriche, O. Aleveque, P. Frere and J. Roncali, *J. Am. Chem. Soc*., 2006, **128**, 3459;
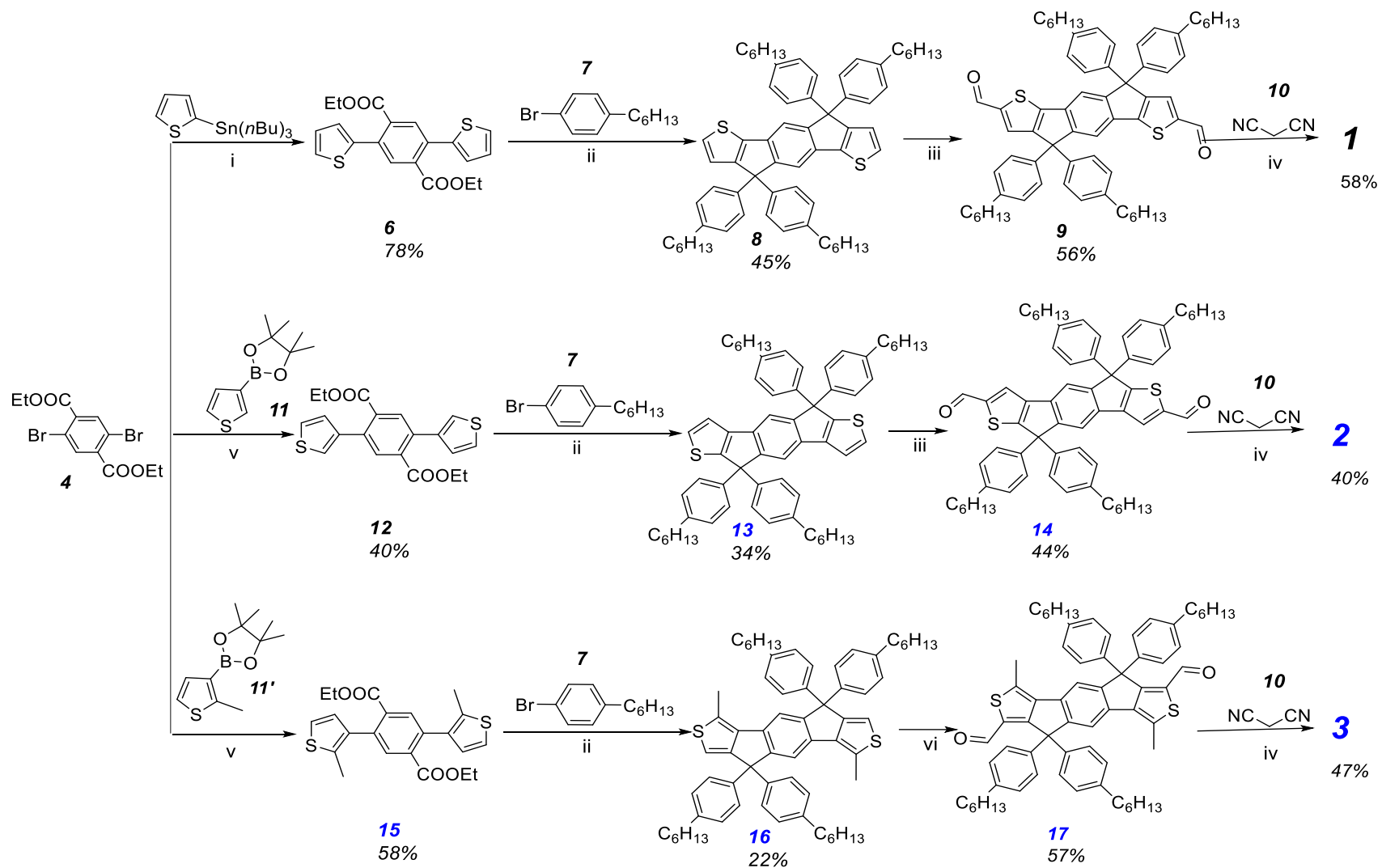
**Scheme 1.** Synthetic route to compounds *1*, *2* and *3*: i) dry toluene, Pd(PPh$_3$)$_4$, 100°C, 24 h; ii) dry THF, *n*BuLi, -78°C; AcOH/H$_2$SO$_4$, reflux, 4 h; iii) 1,2-DCE, POCl$_3$, DMF, 65°C, 12 h; iv) dry toluene, pyridine, reflux; v) toluene, Pd(dppf)Cl$_2$, Cs$_2$CO$_3$, 100°C, 48 h; vi) DCM, TiCl$_4$,Cl$_2$CHOCH$_3$, r.t.

**Table 1**. Experimental optoelectronic data of all three final compounds and of their corresponding intermediates

| CMPD. | UV-VIS DATA | | CYCLIC VOLTAMMTRY | |
|---|---|---|---|---|
| | In CH$_2$Cl$_2$ sol. ($\lambda$ [nm]) | Thin films ($\lambda$ [nm]) | E$_{pa}$ (V) | E$_{pc}$ (V) |
| *8* | 348, **366** | 336, 353, **372** | 0.73, 1.00 | -1.15 |
| *9* | 408, **430** | 413, **438** | - | -1.40 |
| *1* | 495, **528** | 502, **528** | 1.39 | -0.93, -1.14 |
| *13* | 319, **333** | 321, **336** | 1.14 | -1.07 |
| *14* | 306, 327, **373** | 313, 331, **373** | 1.4 | - |
| *2* | 328, 344, **450** | 330, 346, **451** | 1.47 | -1.15 |
| *16* | 330, 337, **344** | 331, 340, **348** | 1.19 | -0.96 |
| *17* | 305, 320, **370** | 303, 320, **375** | 1.43 | - |
| *3* | 309, 371, **426** | 342, 388, **444** | 1.49 | -1.35 |
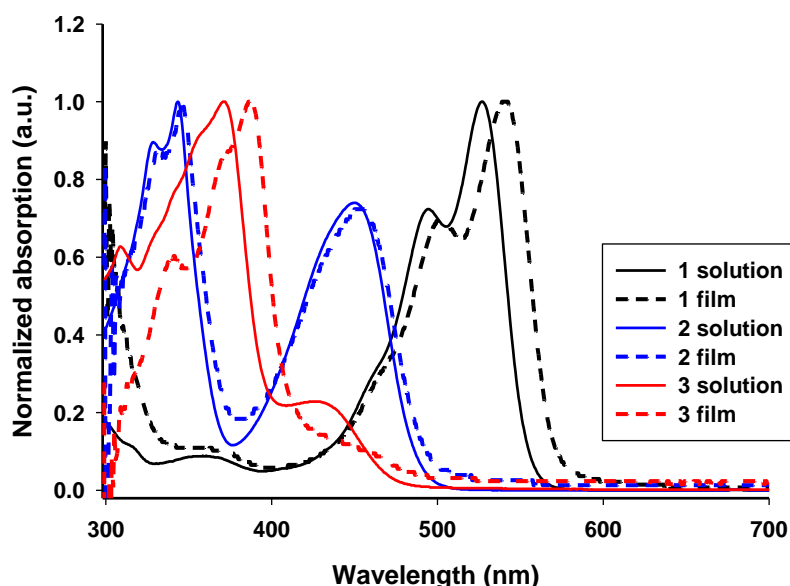


**Figure 3.** UV-Vis absorption spectra of compounds *1* (black)**,** *2* (blue) and *3* (red) in DCM solution (solid line) and film spin-cast on glass (dotted)

The electrochemical properties of all the compounds have been investigated by cyclic voltammetry (CV) in dichloromethane solution using Bu$_4$NPF$_6$ as supporting electrolyte. The CV data of intermediate derivatives (IDT cores (*8*, *13* and *16*) with their corresponding dialdehyde (*9*, *14* and *17*)) are summarized in table 1.

The HOMO and LUMO energy levels were determined using the onset of the oxidation and the reduction processes and compared with theoretical optimized data (table 2).
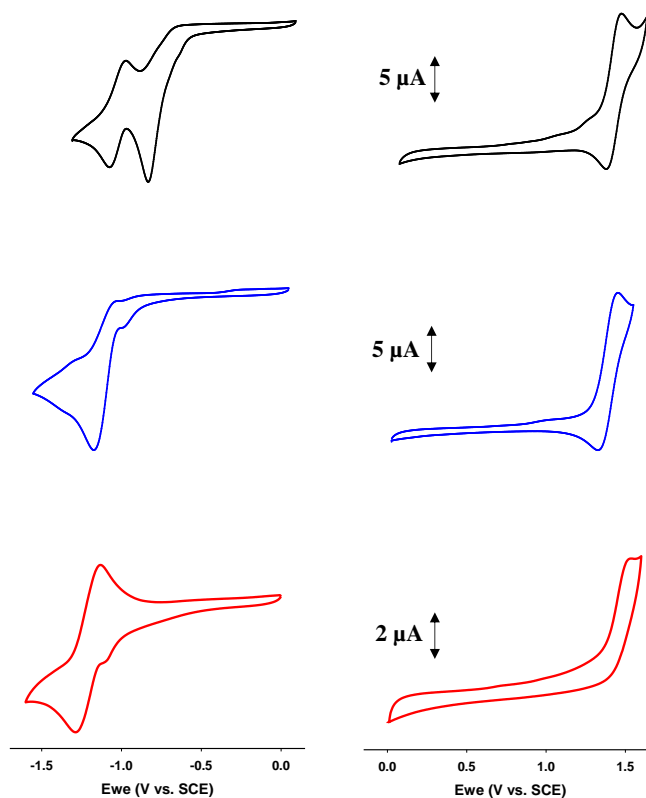
**Figure 4.** Cyclic voltammogram of compound **1** (top), **2** (middle) and **3** (bottom) in DCM solution of 0.1 M Bu$_4$NPF$_6$ with scan rate 100 mV/s, Pt electrodes, ref. *SCE*

### 2.1.1.4.Theoretical calculations

In order to a better understanding of the electronic structure and the geometry of the target compounds, quantum chemical calculations based on density functional methods have been performed. The theoretical data are in agreement with those obtained by experimental and ll data are summarized in table 2.

**Table 2.** Experimental and theoretical optoelectronic properties

| Cmpd. | Experimental[a] | | | Theoretical[b] | | |
|---|---|---|---|---|---|---|
| | $E_{HOMO}$ (eV) | $E_{LUMO}$ (eV) | ΔE (eV) | $E_{HOMO}$ (eV) | $E_{LUMO}$ (eV) | ΔE (eV) |
| *1* | -5.91 | -3.88 | 2.03 | -5.86 | -3.31 | 2.55 |
| *2* | -5.99 | -3.78 | 2.21 | -5.93 | -2.93 | 3.00 |
| *3* | -6.02 | -3.72 | 2.30 | -5.98 | -2.81 | 3.18 |

[a]from the onset of oxidation and reduction waves using an offset of -4.68 eV
[b]from optimized geometries

### 2.1.2. Acceptors and donors based on indaceno[1,2-b:5,6-b']dithiophene

We found that the system based on the **IDT-1** core exhibited the best optoelectronic properties, hence we decided to synthesize and investigate new A-D-A assemblies, owning **IDT-1** core, in order to evaluate the potential of these compounds as *p*- and *n*-type

semiconductor materials in bulk heterojunction organic solar cells (BHJ OSCs). The photovoltaic properties of obtained compounds were investigated in inverted solar cells configuration and are discussed as concerns the structure-property relationship.

### 2.1.2.1. Synthesis of compounds

The compounds presented in this chapter are based on indacenodithiophene as central core and various end-capping units originated from 3-ethyl-2 thioxothiazolidin-4-one *18*, 2-(ethylthio)thiazol-4(5*H*)-one *19*, 1,1-dicyanomethylene-3-indanone *20*, *21*, and 2-benzofuran *22* (figure 5).
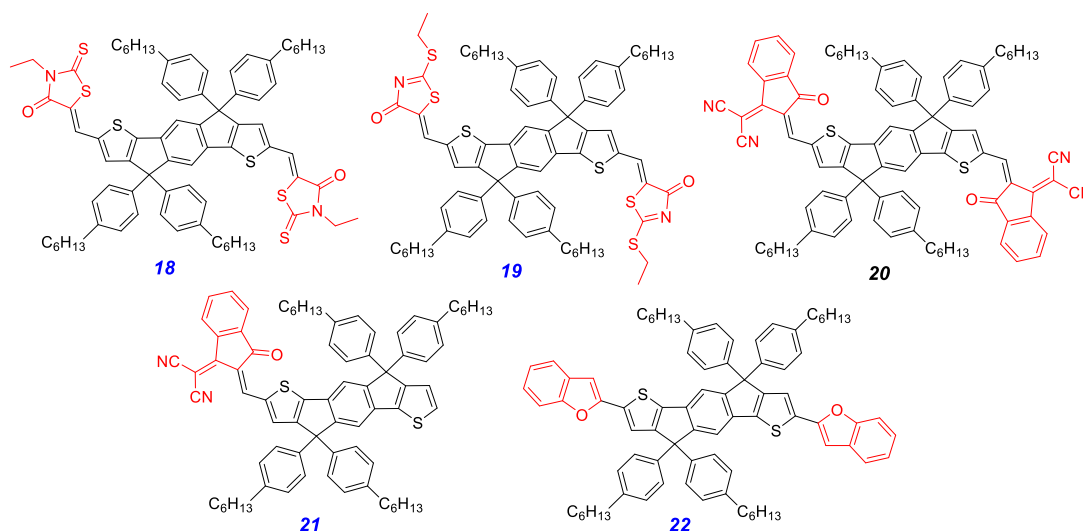


**Figure 5.** The chemical structure of target compounds *18-22*
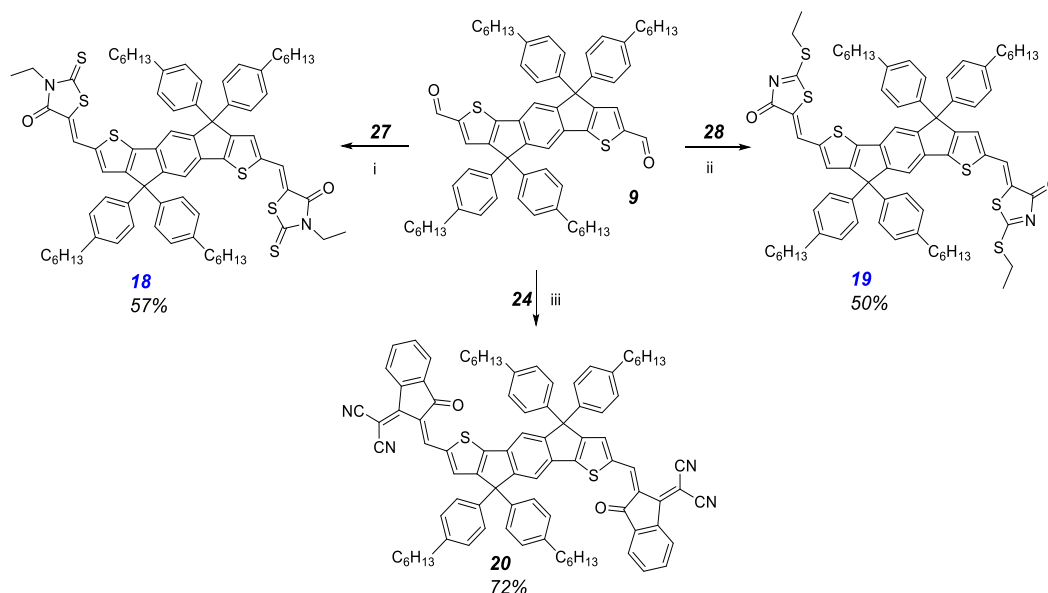


**Scheme 2.** Synthesis of target compounds *18-20*; i) toluene, pyridine, 65°C, 18 h; ii) toluene, pyridine, 65°C, 20 h; iii) toluene, pyridine, 65°C, 8 h.

The target compounds *18*, *19* and **20** were obtained by Knoevenagel condensation reaction of aldehyde *9* with the corresponding electron-acceptor moieties (scheme 2). The compounds were purified through column chromatography and were obtained in 50-72% yields.

For the investigation of the symmetry impact of molecules on electronic properties of compounds, a new nonsymmetric structure was designed and synthesized. Therefore, starting from compound *8* the monoformylated compound *8'* was obtained and further used in a Knoevenagel condensation with indandione derivative *24* to get the nonsymmetric D-A compound *21* (scheme 3).

Also, a new D-A-D type donor was designed and obtained by using IDT core as acceptor unit and a 2-benzofuran derivative as donor terminal groups (scheme 4). Compound *30* was synthesized by a lithiation reaction of benzofuran *29* with tributylchlorostannane. Derivative *31* was obtained as a result of bromination reaction of compound *8* with NBS. For the access to compound *22*, a Stille coupling reaction was done between benzofuran derivative *30* and dibrominated intermediate *31*.
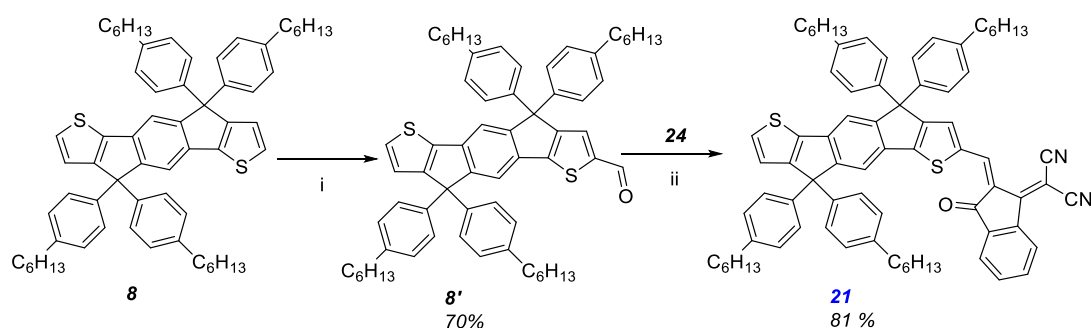


**Scheme 3.** Synthesis of compound *21*; i) POCl$_3$, DMF, 1,2-DCE, 65°C, overnight ii) toluene, pyridine, 65°C, 3 h.
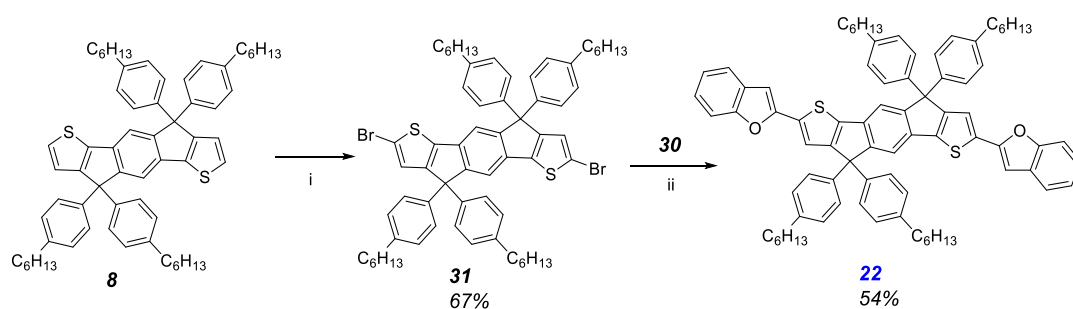


**Scheme 4.** Synthesis of *22*: i) CHCl$_3$, NBS, rt, 15 h; ii) dry toluene, Pd(PPh$_3$)$_4$, 100°C, 24 h

### 2.1.2.2. Optical and electrochemical properties

The optoelectronic properties of the target compounds were investigated by UV-Vis and cyclic voltammetry. The absorption properties were investigated both in solution and thin films spun-cast on glass. The UV-Vis spectra recorded in dichloromethane solutions have almost the same profiles for all compounds displaying strong absorption bands in the 430-650 nm region (figure 6, second row, left). The absorption spectra of thin films spun-cast on glass exhibit also a red shift of absorption maximum with respect to their corresponding solution spectra (figure

6, second row, right). Comparing the electronic properties of these acceptors a red shift of absorption maxima can be observed started from compound *1* and *19* to compound *18* and then to compound *21* and *20* (table 3). The replacement of the acceptor moieties with a 2-benzofuran unit led to a hypsochromic shift of the $\lambda_{max}$ (not shown).
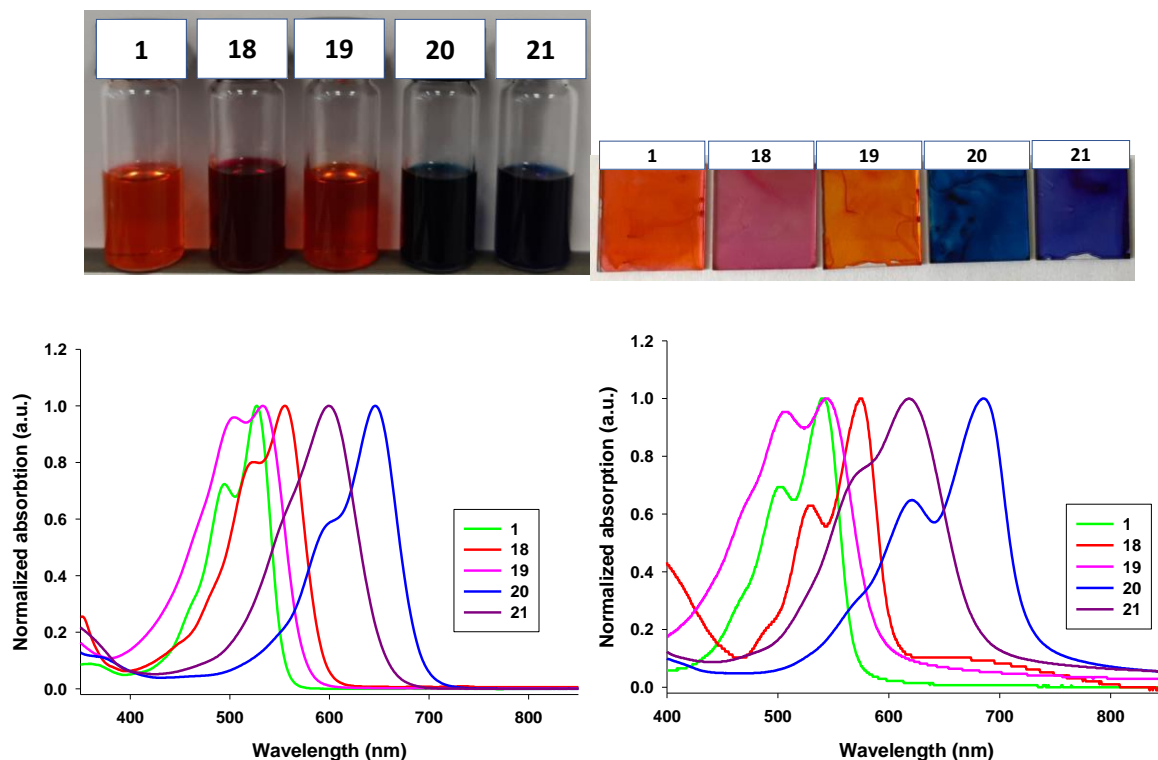


**Figure 6.** The solution and thin films spun-cast on glass (first row); normalized absorption spectra in solution (second row, left) and thin film spin-coated on glass (second row, right) of acceptors *1*, *18-21*

**Table 3.** Experimental Optoelectronic data of IDT compounds

| CMPD. | UV-VIS DATA | | CYCLIC VOLTAMMETRY | |
|---|---|---|---|---|
| | In CH$_2$Cl$_2$ solution (λ(nm)) | Thin films (λ (nm)) | E$_{pa}$ (V) | E$_{pc}$ (V) |
| *1* | 495, **527** | 502, **540** | 1.40 | -0.92, -1.17 |
| *18* | 523, **555** | 530, **576** | 1.22 | -1.13 |
| *19* | 505, **533** | 506, **544** | 1.22 | -1.32 |
| *20* | 598, **645** | 620, **686** | 1.42 | -0.71, -0.89 |
| *21* | **595** | 568, **619** | 0.87, 1.12 | -1.08, -0.82 |
| *22* | 430, **455** | 436, **462** 439, **473*** | 0.88, 1.20 | - |
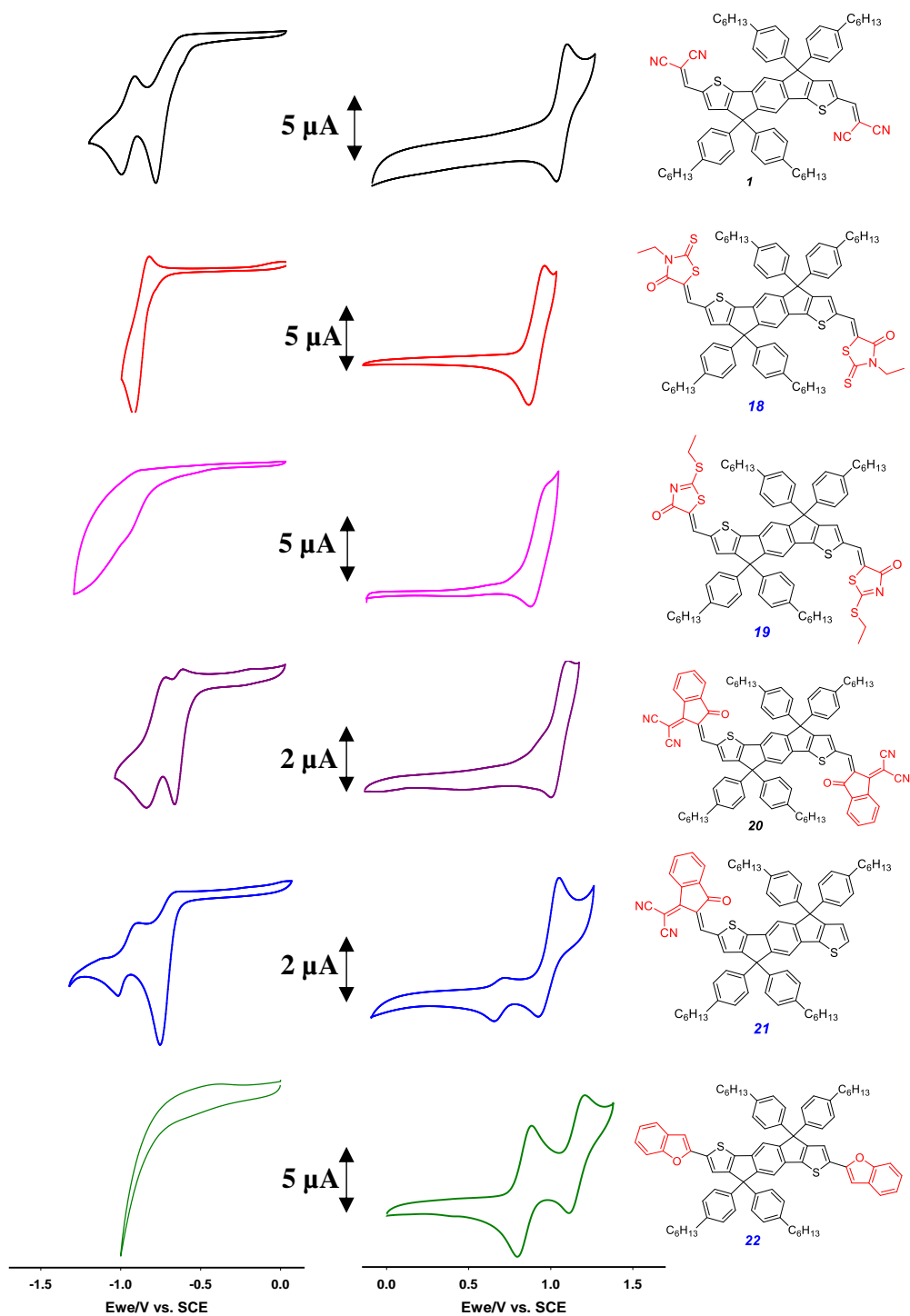
**Figure 7.** Cyclic voltammograms of compounds *1*, *18-22* in 0.10 M Bu$_4$NPF$_6$/CH$_2$Cl$_2$, Pt electrodes, scan rate 100 mV s$^{-1}$, ref *SCE*

The electrochemical properties of the compounds were analyzed by cyclic voltammetry (CV) in methylene chloride, in presence of 0.1M Bu$_4$NPF$_6$ as supporting electrolyte (table 3, figure 7). The highest occupied molecular orbital (HOMO) and the lowest unoccupied molecular orbital (LUMO) levels were determined from the onset of the oxidation process using an offset of -4.68 eV for *SCE vs* the vacuum level.

### 2.1.2.3.Theoretical calculations

In order to assess a better understanding of the optoelectronic properties of the synthesized IDT derivatives, the HOMO and LUMO orbitals and optimized geometries were calculated and the data are summarized in table 4.

**Table 4.** Calculated and experimental optoelectronic properties of IDT compounds

| | Experimental | | | | Theoretical | | |
|---|---|---|---|---|---|---|---|
| | $E_{HOMO}$ (eV) [a] | $E_{LUMO}$ (eV) [a] | $\Delta E$ (eV) [a] | $\Delta E$ (eV) [b] | $E_{HOMO}$ (eV) | $E_{LUMO}$ (eV) | $\Delta E$ (eV) |
| *1* | -5.91 | -3.88 | 2.03 | 2.13 | -6.00 | -3.47 | 2.53 |
| *18* | -5.68 | -3.60 | 2.05 | 2.04 | -5.60 | -3.22 | 2.38 |
| *19* | -5.66 | -3.62 | 2.01 | 2.10 | -5.52 | -3.04 | 2.48 |
| *20* | -5.86 | -4.00 | 1.77 | 1.70 | -5.86 | -3.65 | 2.21 |
| *21* | -5.45 | -3.60 | 1.85 | 1.79 | -5.69 | -3.36 | 2.33 |
| *22* | -5.44 | -2.86 | 2.58 | 2.53 | -5.16 | -2.30 | 2.86 |

[a]from the onset of oxidation and reduction waves using an offset of $-4.68$ eV for SCE
[b]from the maximum absorption onset in thin films

### 2.1.2.4. Evaluation of the photovoltaic properties

Compounds *1*, *18* - *21* were tested as acceptor materials in inverted bulk heterojunction (BHJ) solar cells using the commercially available regioregular Poly(3-hexylthiophene-2,5-diyl) (P3HT) as donor material, while compound *22* was tested as donor material in devices of same architecture but using $PC_{61}BM$ as acceptor material.

**Table 5.** Photovoltaic characteristics of BHJ OSCs: ITO/ZnO/D/A/MoO₃/Al under AM 1.5 simulated solar light with an incident power light of 100 mW cm⁻

| Donor | Acceptor | D:A ratio (w:w) | $V_{oc}$ [V] | $J_{sc}$ [mAcm⁻²] | FF [%] | *PCE* [%] | Average *PCE* |
|---|---|---|---|---|---|---|---|
| **P3HT** | *1* | 1:2 | 0.67 | 1.76 | 46.32 | 0.55 | 0.52 |
| **P3HT** | *18* | 1:1 | 0.97 | 3.90 | 45.56 | 1.74 | 1.67 |
| **P3HT** | *19* | 1:2 | 0.79 | 0.89 | 41.31 | 0.29 | 0.26 |
| **P3HT** | *20* | 1:1 | 0.54 | 7.23 | 56.53 | 2.21 | 2.11 |
| **P3HT** | *21* | 1:1 | 0.57 | 2.71 | 42.83 | 0.67 | 0.62 |
| *22* | **PC₆₁BM** | 1:2 | 0.94 | 4.03 | 34.29 | 1.30 | 1.2 |

The commercially compounds were selected so that the energy HOMO-LUMO levels are compatible with a photoinduced electron transfer from the HOMO of the donor to the LUMO of the acceptor. The BHJ cells were fabricated using the architecture presented in figure 8 and the obtained results are summarized in table 5.
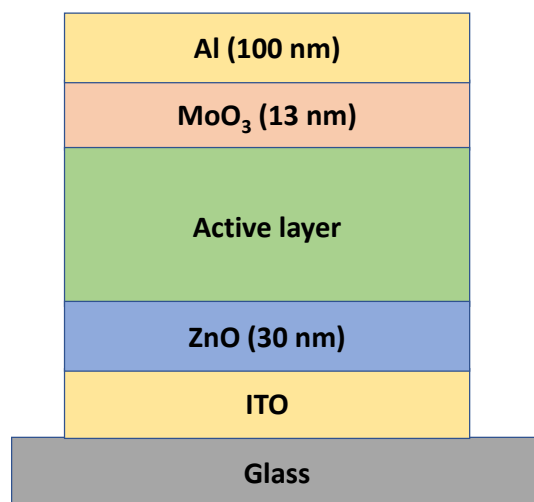


**Figure 8.** The design of the used inverted solar cell devices

## 2.2. *Small donor-acceptor molecules for Single-Material Organic Solar Cells (SMOSCs)*

This chapter describes the synthesis of a series of D- $\pi$ -A type compounds involving a triarylamine unit as donor connected through a thienyl or phenyl spacer to different electron acceptor groups (figure 9). The acceptor moieties are based on 1,3-indandione derivatives such as 2-(2,3-dihydro-3-oxo-1*H*-benz finden-1-ylidene)propanedinitrile (in case of compounds *32*, *35*, *36*) and 2,2′-(1*H*-indene-1,3(2H)-diylidene)bis propanedinitrile (compound *33*) or naphthalene-based derivative 2-(3-oxo-2,3-dihydro-1*H*-cyclopenta bnaphthalen-1-ylidene)malononitrile (in case of compound *34*).[3]
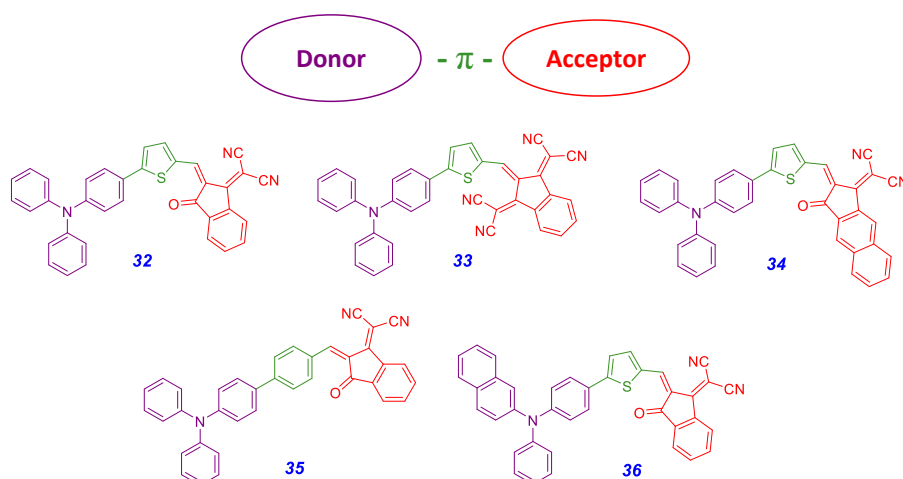


**Figure 9.** Chemical structure of target compounds

[3] N. Terenti, G.-I. Giurgi, A. P. Crişan, C. Anghel, A. Bogdan, A. Pop, I. Stroia, A. Terec, L. Szolga, I. Grosu, and J. Roncali, *J. Mater. Chem. C*, 2022, **10**, 5716;

### 2.2.1. *Synthesis of compounds*

Compounds *32*, *33* and *34* were synthesized in high yield by a simple and facile procedure (scheme 5). The intermediate compounds *38* and *39* were synthesized using a reported procedure , involving a Stille coupling reaction of comercially available 4-bromo-N,N-diphenylaniline *37* and tributyl(thiophen-2-yl)stannane *5* followed by a Vilsmeier formylation reaction. The target compound *32*, *33* and *34* were obtained by a Knoevenagel condensation between coresponding indandione-based acceptor and aldehyde derivative *39* in ethanol the presence of triethylamine (for compounds *32* and *34*) and in acetic anhydride as solvent and catalyst for compound *33*. Another objective of this work was to study the impact of the π spacer of the D- π -A systems regarding the optoelectronic and photovoltaic properties. In order to get compound *35*, a Suzuki cross-coupling reaction of commercially available compounds *37* and *45* was done, followed by a Knoevenagel condensation indandione-based derivative *24* (scheme 6).
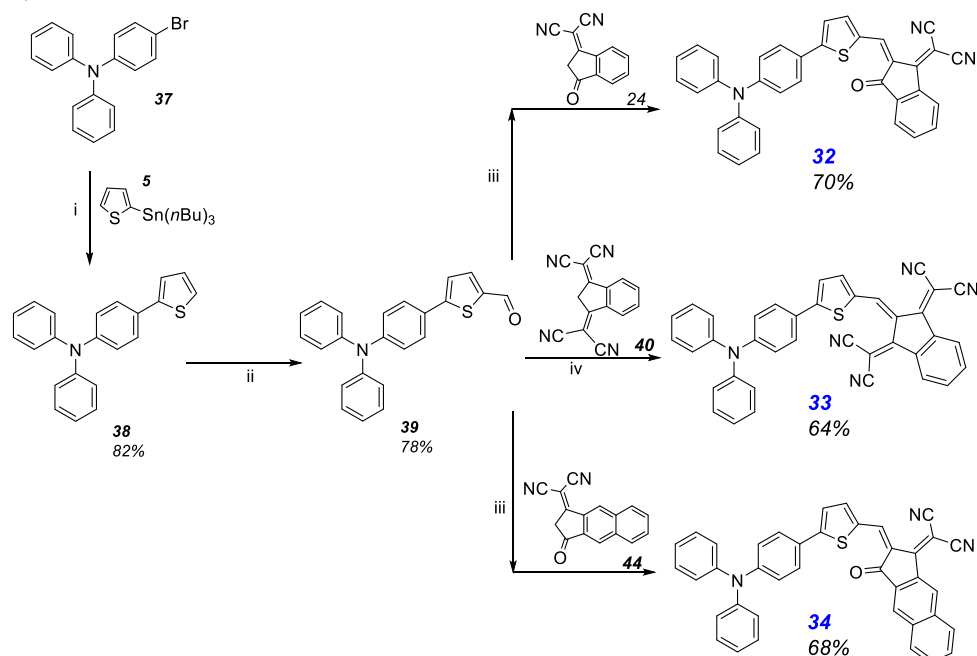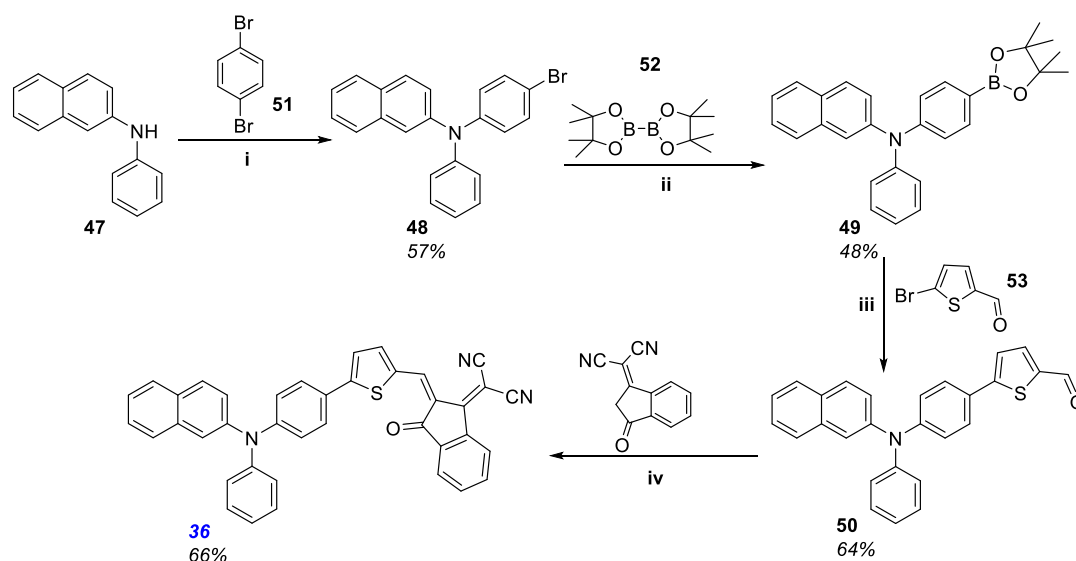
**Scheme 5**. Synthesis of compounds **32 - 34**; i) dry toluene, Pd(PPh$_3$)$_4$, 36 h, reflux; ii) 1,2-DCE, POCl$_3$, DMF, 16 h, 65°C; iii) dry toluene, Et$_3$N, 17 h, 65°C; iv) acetic ahnidride r.t., 2 h
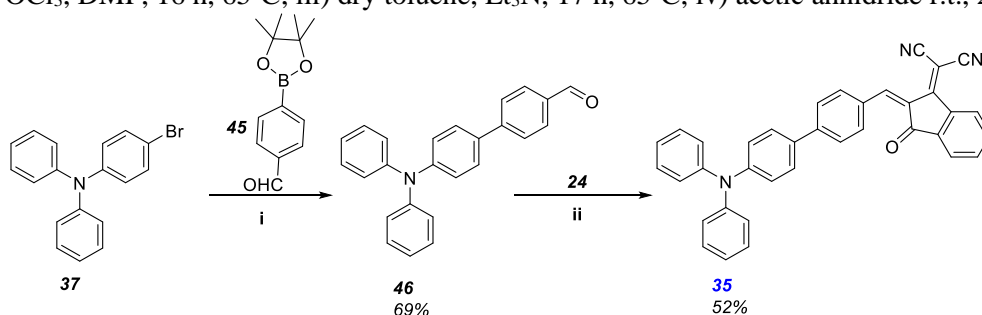
**Scheme 6.** Synthesis of compound **35**; i) DME/H$_2$O, Cs$_2$CO$_3$, Pd(PPh$_3$)$_4$, overnight, 80°C; ii) EtOH, 18 h, 65°C.

In order to analyze the influence of donor's strength on electrochemical properties, one of the phenyl units of derivative *32* was replaced by a *b*-naphthyl moiety. The target compound *36* bearing a *b*-naphthyl moiety was obtained following a multi-step strategy depicted in scheme 7.



**Scheme 7.** Synthesis of compounds **48-50** and *36*; i) dry toluene, NaOᵗBu, Pd(dppf)Cl₂, overnight, reflux; ii) 1,4-dioxane, KOAc, Pd(dppf)Cl₂, overnight, reflux; iii) 1,4-dioxane/H₂O, Cs₂CO₃, Pd(dppf)Cl₂, overnight, reflux; iv) dry toluene, Et₃N, 6 h, 65ºC.

### 2.2.2. *Solid-state investigations*

Dark-blue (*33*, *34*) and dark-orange (*35*) single crystals were obtained from dichloromethane solution by slow evaporation technique. All molecular structures display the usual propeller-like geometry of the TPA block. All three compounds crystallize in the centro-symmetric monoclinic space group with one molecule of TPA derivative per asymmetric unit.

Single crystal molecular structure for compound *33* shows a significant distortion of the entire molecule caused by the two DCV groups on the acceptor block (figure 10). The acceptor moiety is not coplanar with the π spacer unit and forms an angle $\theta_2$ of 12.5º. In the acceptor part, the two dicyanovinyl groups are oriented outwards on the same side of the indene unit plane adopting in this way a butterfly shape.
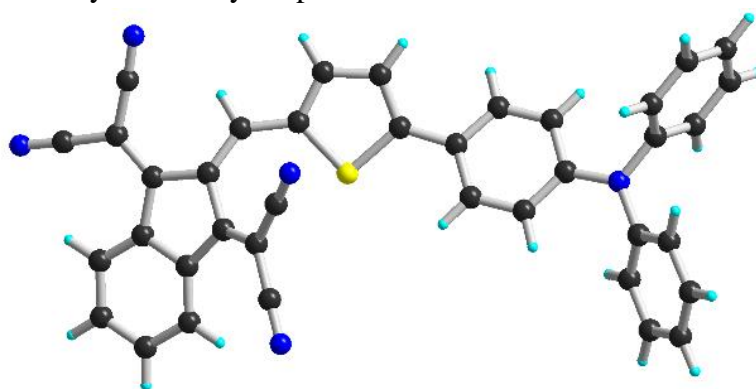


**Figure 10.** Crystal structure of compound *33*

The X-ray analysis of a single crystal of *34* reveals an asymmetric unit involving a single molecule solvated with a DCM molecule (figure 11). The acceptor unit is almost coplanar with the π spacer unit with a dihedral angle $\theta_2$ of 2.5°, while the dihedral angle $\theta_1$ formed by the inner TPA phenyl group and the thiophene ring is 21.1°. In the acceptor block, the inner cyano group forms an angle of 15.1° with the plane of the cyclopenta[*b*]naphthalene unit.
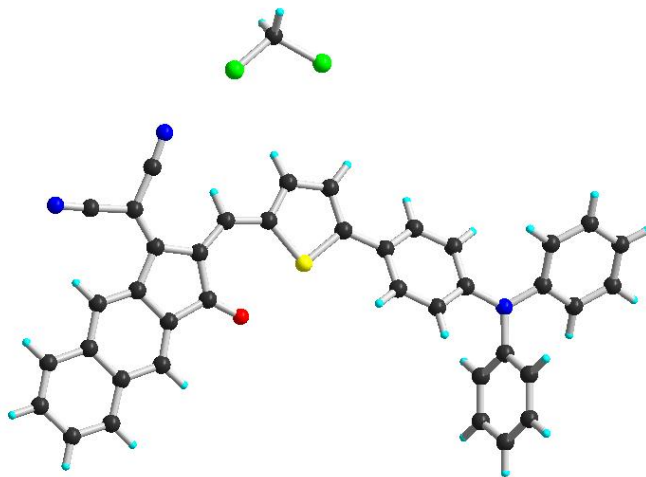
**Figure 11.** Crystal structure of compound *34* with a dichloromethane molecule

In the case of compound *35* in which the thienyl bridge is replaced by a phenyl, X-ray diffraction analysis reveals an angle $\theta_1$ of 21.9° and $\theta_2$ of 4.6° formed by the π spacer unit with the TPA phenyl ring and with the acceptor block respectively (figure 12). Also, the crystallographic structure shows a deviation from planarity for one of the cyano groups, with a 12.3° angle with the plane of the indene unit.
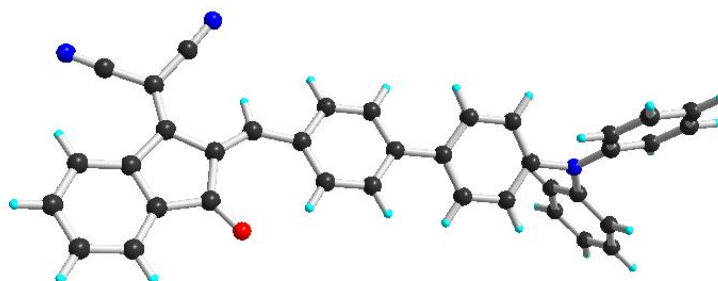
**Figure 12.** Crystal structure of compound *35*

### 2.2.3. *Optical and electrochemical properties*

The optoelectronic properties of the triarylamine compounds decorated with different accepting moieties have been investigated by ultraviolet-visible (UV-vis) spectroscopy, both in dicloromethane solution and as thin film. The UV-Vis absorption spectra of all compounds reveal two or three bands in the 270–450 nm region that can be assigned to the π - π * transition followed by a more intense band in the 500–635 nm region assigned to an internal charge transfer (ICT) transition (figure 13). As expected, the absorption spectra of thin films cast on glass from dichloromethane solutions present a slight red shift of $\lambda_{max}$ and broadening of the absorption band suggesting intermolecular interactions in the solid state.

**Table 6.** Experimental optoelectronic data of target compounds

| COMP. | UV-VIS | | CYCLIC VOLTAMMETRY | |
|---|---|---|---|---|
| | In CH$_2$Cl$_2$ Sol ($\lambda_{max}$ [nm]) | Thin films ($\lambda_{max}$ [nm]) | Epa (V) | Epc (V) |
| *32* | 604 | 625 | 1.00 | -0.79 |
| *33* | 660 | 690 | 1.06 | -0.58 |
| *34* | 635 | 650 | 1.04 | -0.74 |
| *35* | 530 | 585 | 1.04 | -0.82 |
| *36* | 606 | 627 | 1.02 | -0.75 |
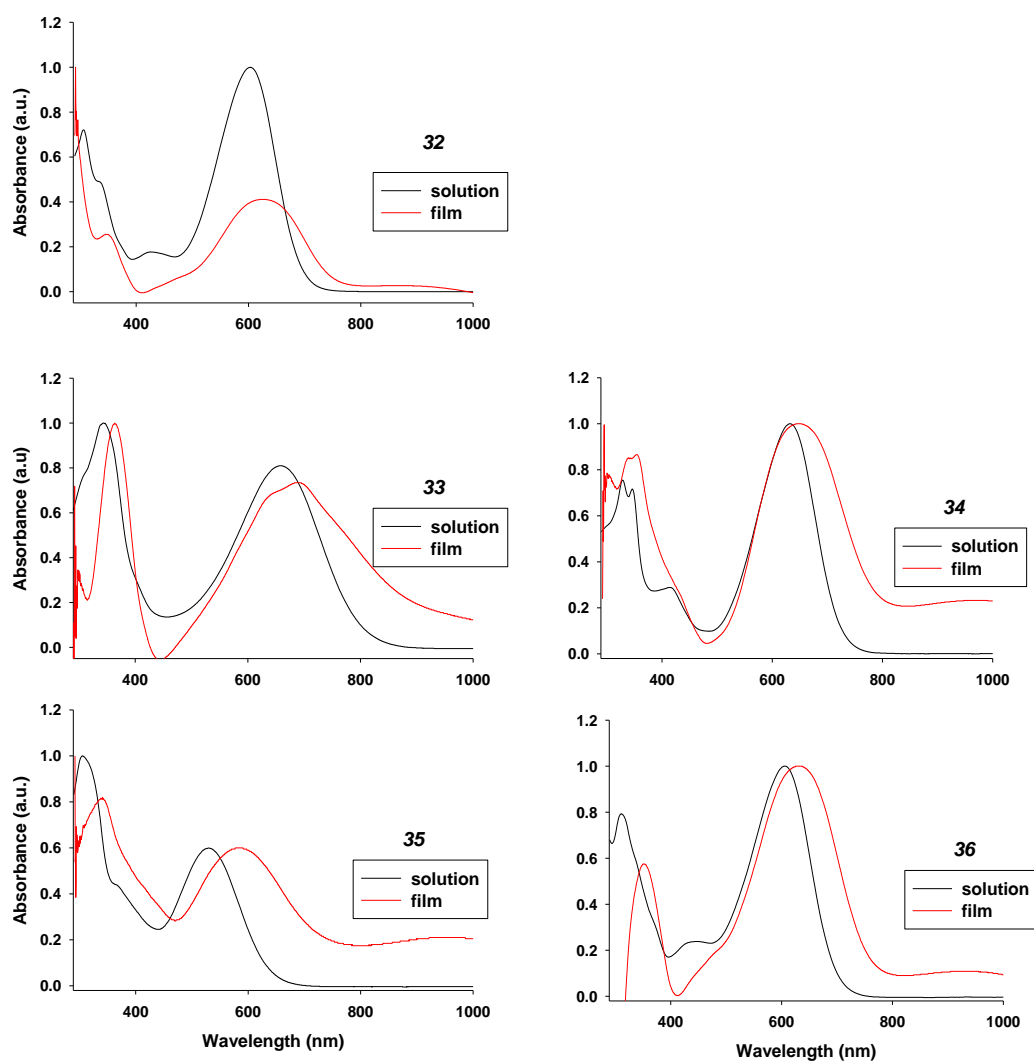


**Figure 13.** Normalized absorption spectra in solution (blak line) and thin film spin-coated on glass (red line) of compounds *32* – *36*

The electrochemical properties of the compounds were analyzed by cyclic voltammetry (CV) in methylene chloride, in presence of 0.1M tetrabutylammonium hexafluorophosphate as supporting electrolyte. All compounds present very similar CV that exhibit a reversible one electron oxidation process with an anodic peak potential ($E_{pa}$) at around 1.00 V *vs SCE* corresponding to the formation of the cation-radical and an irreversible reduction process with a cathodic peak potential ($E_{pc}$) in the -0.58 to -0.82 V region (table 6, figure 14). These results are in agreement with optical data and confirm that the HOMO of the compounds is determined by the TPA donor block while the LUMO level, the HOMO-LUMO gap ($\Delta E$) are controlled by the nature of the acceptor groups.
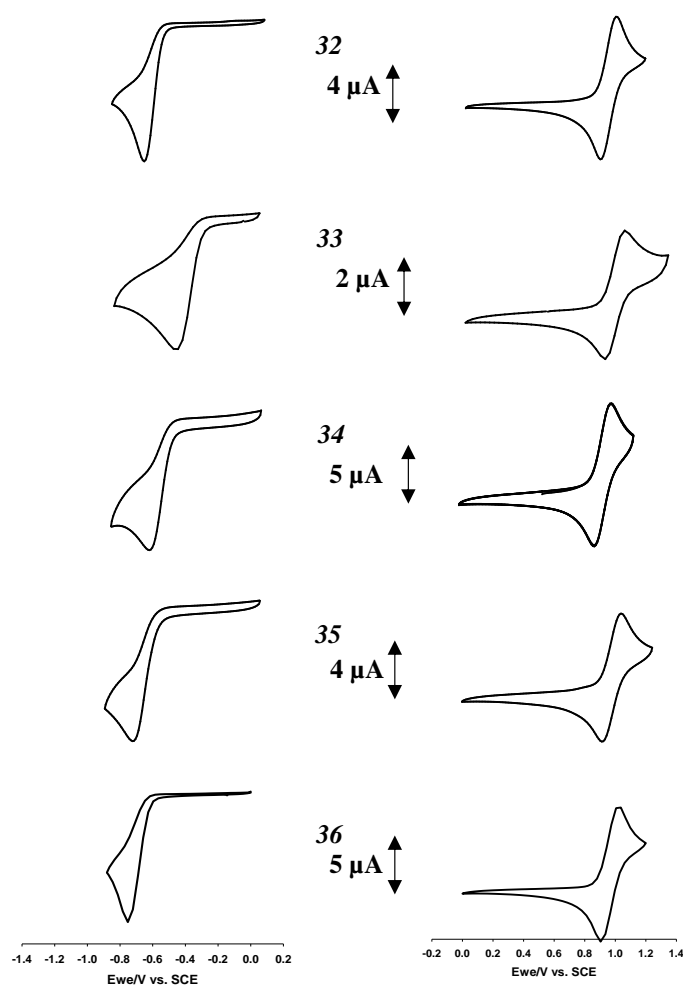


**Figure 14.** Cyclic voltammograms of compounds *32* - *36* in 0.10 M Bu$_4$NPF$_6$/CH$_2$Cl$_2$, Pt electrodes, scan rate 100 mV s$^{-1}$, ref. *SCE*

### *2.2.4.Theoretical calculations*

Density functional theory (DFT) calculations at the B3LYP/6- 31G(*d*) level were also performed to investigate the chemical geometry of compounds *32* - *36*. The optimized structures of the molecules are in agreement with X-ray data. The theoretical and experimental HOMO and LUMO levels are summarized in table 7.

**Table 7**. Calculated and experimental electronic properties of TPA compounds

| | Experimental | | | Theoretic | | |
|---|---|---|---|---|---|---|
| | $E_{HOMO}$ (eV) | $E_{LUMO}$ (eV) | $\Delta E$ (eV) | $E_{HOMO}$ (eV) | $E_{LUMO}$ (eV) | $\Delta E$ (eV) |
| *32* | -5.54 | -4.03 | 1.55 | -5.44 | -3.34 | 2.10 |
| *33* | -5.56 | -4.28 | 1.38 | -5.51 | -3.51 | 2.00 |
| *34* | -5.58 | -4.08 | 1.57 | -5.45 | -3.40 | 2.05 |
| *35* | -5.58 | -4.02 | 1.69 | -5.40 | -3.37 | 2.03 |
| *36* | -5.53 | -4.08 | 1.60 | -5.42 | -3.34 | 2.08 |

### 2.2.4. *Evaluation of the photovoltaic properties*

The photovoltaic performances of compounds *32* - *36* as single material, were determined in both the direct and inverted configuration using architecture of solar cells presented in figure 15. The results obtained in direct configuration are in agreement with those obtained in inverted configuration (table 8) for all compounds and are related to the chemical structures of the molecules. Comparing the results obtained for compounds *32* and *34*, that differ by acceptor unit contrary to our expectation, a large decrease of $J_{sc}$ and *PCE* for both types of cells was observed for compound *34*. Due to the fragility of compound *34*, an inverted cell based on spin-cast film was fabricated and the results confirm that a much higher efficiency is obtained.

**Table 8.** Photovoltaic characteristics for SMOSCs based on *32* - *36* under AM 1.5 simulated solar light with a power light intensity of 100 mW cm$^{-2}$ (* spin-cast from chloroform solution)

| Active layer/ compound | Cell type | $V_{oc}$ [V] | $J_{sc}$ [mAcm$^{-2}$] | FF [%] | *PCE* [%] | Average *PCE* |
|---|---|---|---|---|---|---|
| *32* | direct | 0.73 | 1.49 | 33.9 | 0.46 | 0.43 |
| | inverted | 1.05 | 3.49 | 23.6 | 0.86 | 0.82 |
| *33* | direct | 0.35 | 0.46 | 36.0 | 0.06 | 0.05 |
| | inverted | 0.49 | 0.75 | 25.9 | 0.10 | 0.09 |
| *34* | direct | 0.70 | 0.81 | 28.2 | 0.16 | 0.10 |
| | inverted | 0.78 | 2.41 | 26.5 | 0.42 | 0.49 |
| | inverted* | 0.93 | 3.28 | 26.6 | 0.88 | 0.82 |
| *35* | direct | 1.09 | 0.99 | 30.1 | 0.33 | 0.30 |
| | inverted | 1.05 | 2.18 | 24.3 | 0.57 | 0.52 |
| *36* | direct | 0.90 | 1.57 | 33.7 | 0.48 | 0.45 |
| | inverted | 1.03 | 3.50 | 24.1 | 0.87 | 0.83 |
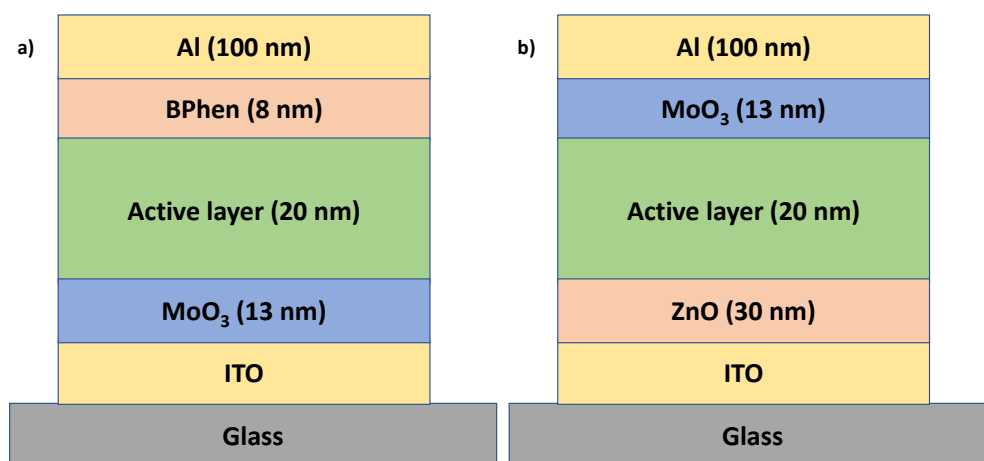
**Figure 15.** The design of direct (a) and inverted (b) solar cells, where the active layer is the one of the compounds *32* - *36*

Compound *33* shows poor performances for both types of cells due to its acceptor unit. The results obtained for *35* show a decrease of the $J_{sc}$ and *PCE* values. Also, by replacing a phenyl with a *β*-naphthyl group in donor unit of compound *36*, there is no improvement as was expected compared to *32*.

*Conclusions*

The cyclic voltammetry and UV-Vis spectroscopy of the three isomers of indacenodithiophene (IDT) (compounds *1*, *2* and *3*) revealed an increasing of the optical band gap from 2.21 eV (compound *1*) to 2.67 eV (compound *3*) and of the LUMO level from -3.88 eV (compound *1*) to -3.72 eV (compound *3*) as result of the modification of the internal charge transfer.

The comparative studies of compounds *1* and *18* - *22*, based on indaceno[*1,2-b:5,6-b'*]dithiophene (**IDT-1**) core and various end-capping units showed a wide range of absorption maxima bands (430 – 650 nm) and energy gaps (2.03 – 2.58 eV). These values are correlated to the strength of the electron-withdrawing groups and reveal the acceptor behavior for compounds *1*, *18* - *21* and the donor behavior for *22*.

Five small D-A molecules exhibiting triphenylamine (compounds *32* - *35*) or *β*-naphthyl diphenylamine (compound *36*) as donor blocks, different acceptors units and aromatic conjugating bridges (thiophene and phenyl) were designed and investigated as SMOSCs. Despite the quite low *PCE* values (which range from 0.1 to 0.88 %) these are among the highest obtained for such simple molecules acting as SMOSCs. The compounds present very similar cyclic voltammograms that exhibit a reversible one electron oxidation process with an anodic peak potential ($E_{pa}$) at around 1.00 V and an irreversible reduction process with a cathodic peak potential ($E_{pc}$) in the -0.58 to -0.82 V region. Replacement of the thienyl spacer by the phenylene one produces a blue shift of $\lambda_{max}$ and a negative shift of $E_{pc}$ (from 0.79 to 0.82 eV).

## Part II: Contributions to Porous Aromatic Frameworks (PAFs) and heterogeneous catalysis

### 1. A short introduction on porous aromatic frameworks

Porous aromatic frameworks (PAFs) stand out by their high surface areas, open architectures, robust skeletons, and excellent stability. Among other remarkable applications of PAFs their use as heterogeneous catalysts, thanks to their ability to entrap various metals or metal-ions within their cavities. Because of their structural features PAFs are able to catalyse different types of reactions in a high yield and to be reused several times without undergoing changes in their structure or to give lower yields.[4,5]

### 2. Original contribution in heterogeneous catalysis

In this context we were interested in the synthesis, characterization and investigation of the catalytic properties of two porous materials based on aromatic building blocks with tetrahedral geometry, namely **PAF-1** and **PAF-2.** The target PAFs were designed to be obtained by Sonogashira cross-coupling reaction, bearing in mind that the copper (I) and palladium (II) pre-catalysts used in their synthesis could be entrapped within the PAFs structure. If so, the new materials should act as heterogeneous catalyst in palladium catalysed cross-coupling reactions and in copper-catalyzed reactions such as: Suzuki-Miyaura cross-coupling, Stille cross-coupling, Copper catalyzed Azide-alkyne cycloaddition (CuAAC), *click* reaction, Huisgen reaction and Sonogashira cross-coupling reaction.

### 2.1. Synthesis and characterization of new PAFs

**PAF-1** and **PAF-2** were obtained by Sonogashira cross-coupling reaction between 1,6-diethynylpyrene[6] (linear linker) and 2,2',7,7'-tetramethoxy-3,3',6,6'-tetraiodo-9,9'-spirobifluorene[7] for **PAF-1** or 1,3,5,7-tetrakis($p$-iodophenyl) adamantane[8] for **PAF-2** (tetrahedral units) in the presence of Pd(PPh$_3$)$_2$Cl$_2$/ CuI co-catalysts. During the PAFs synthesis, the Pd(II) complex was at least partly reduced at catalytically active Pd(0) complex , most probably in presence of the excess of dialkyne (1,6-diethynylpyrene) and trapped as fine nanoparticles into confined spaces of the organic network. The synthesis and simplified representation of the obtained materials are presented in scheme 1. The novelty and the most challenging part of this research is that palladium and cooper (pre)catalysts used to promote the synthesis of PAFs to self-entrap in sufficient amount in their structure, generating in this way PAF-entrapped Pd/Cu catalysts, in order to be directly used for further catalytic applications without any post-synthetic.

[4] L. -P. Jing, J. -S. Sun, F. Sun, P. Chen and G. Zhu, *Chem. Sci.,* 2018, **9**, 3523;

[5] Q. Meng, Y. Huang, D. Deng, Y. Yang, H. Sha, X. Zou, R. Faller, Y. Yuan and G. Zhu, *Adv. Sci.*, 2020, **7**, 2000067;

[6] S. Leroy-Lhez and F. Fages, *Eur. J. Org. Chem.,* 2005, 2684;

[7] L. Pop, F. Dumitru, N. D. Hadade, Y.-M. Legrand, A. van der˜Lee, M. Barboiu and I. Grosu, *Org. Lett.*, 2015, **17**, 3494;

[8] W. Lu, D. Yuan, D. Zhao, C.I. Schilling, O. Plietzsch, T. Muller, S. Bräse, J. Guenther, J. Blümel, R. Krishna, Z. Li and H.-C. Zhou, *Chem. Mater.,* 2010, **22**, 5964;
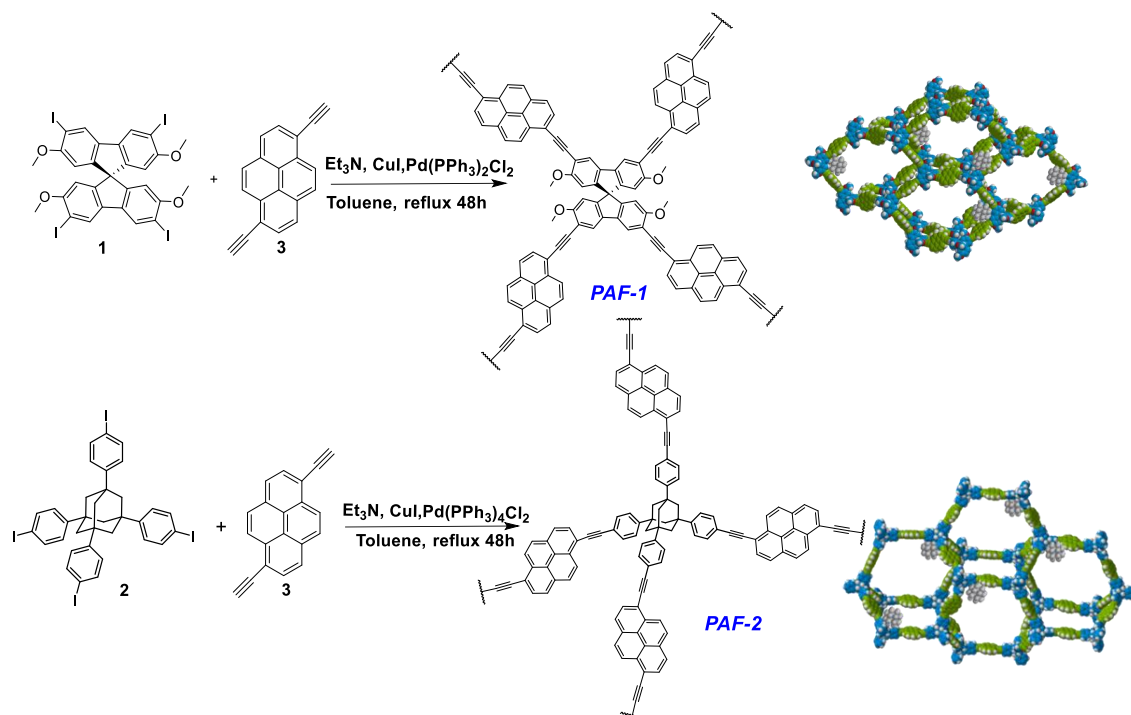
**Scheme 1.** The synthesis of *PAF-1* and *PAF-2* and their schematic representations.

## 2.2. *Catalytic properties of PAFs*

### 2.2.1. *Catalysts for Suzuki-Miyaura cross-coupling reactions*

Based on the observation of entrapped palladium within the frameworks, we set to study the use of *PAF-1* and *PAF-2* as heterogeneous catalysts in Suzuki-Miyaura cross-coupling reactions. The reaction conditions were optimized for the synthesis of *12*. It is worth mentioning that compound *12* could be obtained in similar yield (*i.e.*, 94% conversion after a 16 h reaction time) using the same amount of catalyst *PAF-2* (20 mg) and 0.082 mmol of *p*-cyanophenyl bromide and on ten times larger scale (0.82 mmol of *p*-cyanophenyl bromide).

**Table 1.** Suzuki−Miyaura Coupling Reactions in the Presence of *PAF-1*, *PAF-2* and Pd(PPh₃)₄



| | Boronic derivative | | Organohalide cmpd. | | | |
|---|---|---|---|---|---|---|
| | X | R₁ | R₂ | Prd | Employed catalyst | C (%)ᵃ |
| 1 | OH, B, OH | --CH₃ *4* | --CN *7* | *12* | *PAF-1* | 98 |
| 2 | | | | | *PAF-2* | 96 |

| | | R1 | R2 | Product | Catalyst | C (%) |
|---|---|---|---|---|---|---|
| 3 | [boronic acid $B(OH)_2$] | --CH$_3$ **4** | --CHO **8** | **13** | *PAF-1* | 96 |
| 4 | | | | | *PAF-2* | 96 |
| 5 | [boronic acid $B(OH)_2$] | --CH$_3$ **4** | --CH$_3$ **9** | **14** | *PAF-1* | 98 |
| 6 | | | | | *PAF-2* | 92 |
| 7 | [boronic acid $B(OH)_2$] | --CH$_3$ **4** | --OCH$_3$ **10** | **15** | *PAF-1* | 49 |
| 8 | | | | | *PAF-2* | 47 |
| 9 | [boronic acid $B(OH)_2$] | --CH$_3$ **4** | --H **11** | **16** | *PAF-1* | 74 |
| 10 | | | | | *PAF-2* | 66 |
| 11 | [boronic acid $B(OH)_2$] | --CHO **5** | --CN **7** | **17** | *PAF-1* | 100 |
| 12 | | | | | *PAF-2* | 91 |
| 13 | [pinacol boronate] | --CHO **6** | **7** --CN | **17** | *PAF-1* | 89 |
| 14 | | | | | *PAF-2* | 89 |



Reaction scheme:

R$_1$-C$_6$H$_4$-X  +  R$_2$-C$_6$H$_4$-Br  →[Pd(PPh$_3$)$_4$, Cs$_2$CO$_3$, DME/H$_2$O]  R$_2$-C$_6$H$_4$-C$_6$H$_4$-R$_1$  **(12 - 17)**

| | | R1 | R2 | Product | Catalyst | C (%) |
|---|---|---|---|---|---|---|
| 15 | [boronic acid $B(OH)_2$] | --CH$_3$ **4** | --CN **7** | **12** | Pd(PPh$_3$)$_4$ | 92 |
| 16 | [boronic acid $B(OH)_2$] | --CH$_3$ **4** | --CHO **8** | **13** | Pd(PPh$_3$)$_4$ | 88 |
| 17 | [boronic acid $B(OH)_2$] | --CH$_3$ **4** | --CH$_3$ **9** | **14** | Pd(PPh$_3$)$_4$ | 84 |
| 18 | [boronic acid $B(OH)_2$] | --CH$_3$ **4** | --OCH$_3$ **10** | **15** | Pd(PPh$_3$)$_4$ | 45 |
| 19 | [boronic acid $B(OH)_2$] | --CH$_3$ **4** | --H **11** | **16** | Pd(PPh$_3$)$_4$ | 64 |
| 20 | [boronic acid $B(OH)_2$] | --CHO **5** | --CN **7** | **17** | Pd(PPh$_3$)$_4$ | 65 |
| 21 | [pinacol boronate] | **6** | --CN **7** | **17** | Pd(PPh$_3$)$_4$ | 66 |

C (%) - conversion of the brominated derivative in the desired cross-coupled product.

We also investigated the influence of electronic effect of *p*-substituent on halide compounds to its conversion into the desired cross-coupled product using both boronic acids

and pinacol boronic esters as coupling partners and **PAF-1**, **PAF-2** and Pd(PPh₃)₄ as catalysts (Table 1). As expected, the best results were obtained for substrates with electron-withdrawing substituents at the *para* position to bromine atoms (CN, CHO, entries 1-4 and 7, 8 in Table 1). The conversion of these bromo-derivatives into the expected cross-coupled product exceeds 95% in each chase. On the contrary, the compounds bearing -OCH₃ and H as *p*-substituents led to lower conversion. No palladium leaching was detected in these experiments after recycling the catalysts five times.

### 2.2.2. Catalysts for Stille cross-coupling reaction

Considering the very good results obtained in Suzuki-Miyaura cross-coupling, we decided to use obtained **PAF-1** as catalyst for other cross-coupling reactions.
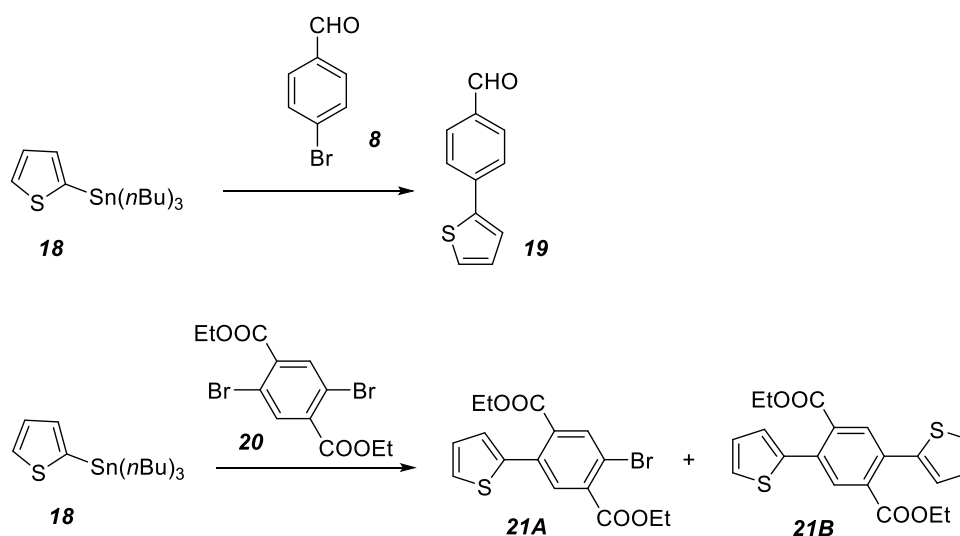


**Scheme 2.** Stille cross-coupling reaction carried out under PAF-1 catalysis, condition: dry toluene, 15 mg **PAF-1**, 24 h, reflux.
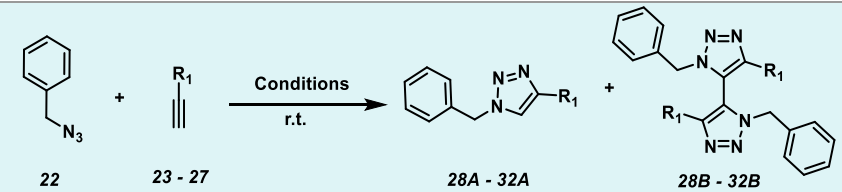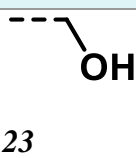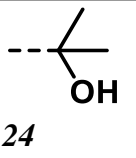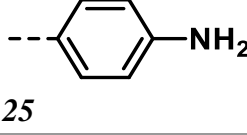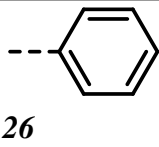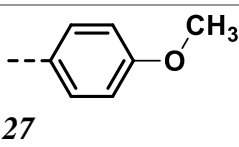
The capacity of **PAF-1** to act as catalyst for Stille reaction was tested using tri-*n*-butyl(thiophen-2-yl) stannane **18** and two different organic halides **8** and **20** (dry toluene, 15 mg **PAF-1**, 24 h, reflux) (scheme 2). Reaction with 4-bromobenzaldehyde **8** yielded compound **19** with a conversion of 52%. The reaction of the same stannane **18** with diethyl 2,5-dibromoterephthalate **20,** under the same condition, led to formation of mono and decoupled products **21A** (26%) and **21B** (23%). The obtained results are preliminary, and show that **PAF-1** can be used as catalyst in Stille coupling, however the reaction conditions should be optimized in order to increase the conversion and to extend the scope of the reaction.

### 2.2.3. Catalysts for Copper(I) Azide-Alkyne Cycloaddition (CuAAC) reactions

The *click* reaction conditions were optimized for the synthesis of **32** (table 2). It is important to mention that the reactions undergo in mild conditions and lead to the formation of 1,4-substituted triazole isomer. With propargyl alcohol or dimethyl ethynyl carbinol as alkyne reagent the reactions were quantitative in both solvents, methanol or water (entries 1-4 in table 2). However, slightly lower conversion was obtained when phenyl-acetylene derivatives with different *para* substituents were used as reactants (entries 5-9 in table 2).

Also, in the case of 4-ethynylaniline **25** and phenylacetylene **26**, when the reactions were performed under air, the formation of a 5,5'-bis-triazole (**B** compound, table 3) by-product together with the expected triazole (**A** product, table 3) in a molar ratio 1:3 was also observed. Total conversion of alkyne **26** into the corresponding 1,4-substituted triazole **31A** and 79% conversion of **25** into triazole **30A** were obtained under argon.

**Table 2.** Alkyne-azide cycloaddition reactions in the presence of **PAF-1**



| | Alkyne | Prod | Condition | | Selectivity ($C^a$(%)): | |
|---|---|---|---|---|---|---|
| | $R_1$ | | Solv. | Atm. | (28-32) A | (28-32) B |
| 1 | (23) OH | 28 | MeOH | Air | Qnt. | - |
| 2 | | | $H_2O$ | Air | Qnt. | - |
| 3 | (24) OH | 29 | MeOH | Air | Qnt. | - |
| 4 | | | $H_2O$ | Air | Qnt. | - |
| 5 | (25) NH₂ | 30 | MeOH | Air | 73 | 27 |
| 6 | | | MeOH | Argon | 79 | - |
| 7 | (26) | 31 | MeOH | Air | 75 | 25 |
| 8 | | | $H_2O$ | Air | Qnt. | - |
| 9 | (27) O CH₃ | 32 | MeOH | Air | 83 | - |

$^a$ C (%) - conversion of the benzyl azide in the **28A-32A** and **28B-32B** products.
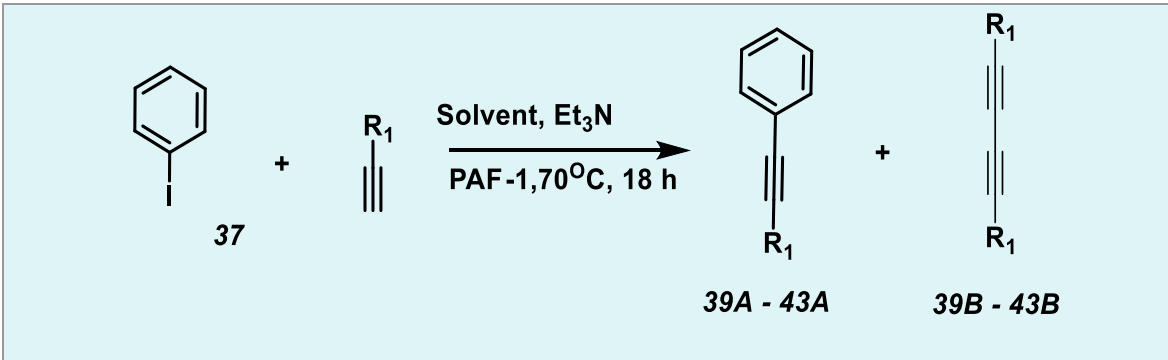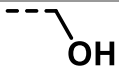
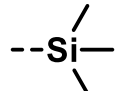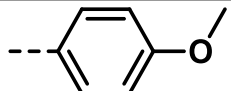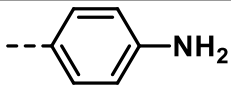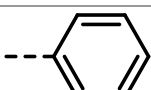### *2.2.4. Catalysts for Sonogashira cross-coupling reactions*

In order to test catalytic activity of **PAF-1** in Sonogashira cross-coupling reaction, iodobenzene was reacted with different alkyne substrates, in molar ratio 1:1. The aliphatic alkynes (propargyl alcohol and ethynyltrimethylsilane) reacted completely with formation of desired cross-coupled products **39** and **40**, without the formation of any by-products (table 3). Moreover, in the case of compound **39**, the reaction was quantitative in both toluene or water

as solvents. Quantitative transformation of alkyne into the cross-coupled product *43* and *40* was also observed when *26* and *38* were used as reactants, respectively.

In the reaction of iodobenzene *37* with 1-ethynyl-4-methoxybenzene *27* and 4-ethynylaniline *25*, the 1,3-diyne compounds (products *41B* and *42B*) were also formed together with the main compound (products *41A* and *42A*) (table 3). Noteworthy, higher conversion into compound *42A* was obtained when water was used as solvent. The conversions were determined from $^1$H-NMR spectra of crude product and were reported as conversion of alkyne derivative into desired compound *A* or by-product *B*. The reaction of *27* with iodobenzene led to the formation of two compounds: the coupled product *41A* and the product formed as result of the alkyne homocoupling *41B*. The formation of two compounds (*42A* and *42B*) was also observed in the reaction of iodobenzene *37* and 4-ethynylaniline *25*.
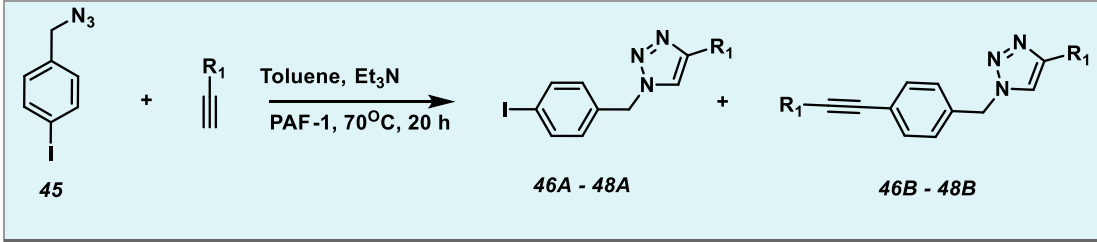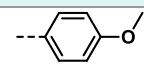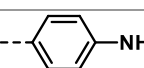
**Table 4.** Sonogashira cross-coupling reactions in the presence of *PAF-1*



| | Alkyne derivative | Product | Solvent | C (%) | |
| | R₁ | | | 39 - 43 A | 39 - 43B |
|---|---|---|---|---|---|
| 1 | OH | *39* | Toluene | Qnt. | - |
| 2 | | | Water | Qnt. | - |
| 3 | --Si— | *40* | Toluene | Qnt. | - |
| 4 | —O | *41* | Toluene | 92 | 8 |
| 5 | —NH₂ | *42* | Toluene | 65 | 35 |
| 6 | | | Water | 89 | 11 |
| 7 | | *43* | Toluene | Qnt. | - |

### 2.2.5. Catalysts for one-pot CuAAC - Sonogashira reactions

The very good results obtained with **PAF-1** as heterogeneous catalyst for both CuAAC and Sonogashira cross-coupling encouraged us to use it to investigate its ability to simultaneously perform these two reactions.

**Table 4:** Sonogashira coupling and click reactions in the presence of **PAF-1**



| | Starting material | | Crude product | | |
|---|---|---|---|---|---|
| | R₁ | Cmpd. | Prod. | C (%) | |
| | | | | 46 – 48 A | 46- 48 B |
| 1 | (phenyl-O) | 27 | 46 | 55 | 45 |
| 2 | (phenyl-NH₂) | 26 | 47 | 66 | 34 |
| 3 | (C(CH₃)₂OH) | 24 | 48 | 53 | 47 |

Therefore, we chose 1-(azidomethyl)-4-iodobenzene as substrate that can react with different terminal alkynes, in 1:2 molar ratio, through iodine group in a Sonogashira cross-coupling and through CuAAC click reactions through the azide group. As experimental reaction conditions we started with the ones that yielded the highest conversions in Sonogashira cross-coupling (toluene as solvent, 20 mg **PAF-1**, 70ºC). The reactions performed under these conditions using a stoichiometric ratio of **45** and alkyne yielded in each case a mixture of compounds (table 4), namely the product of CuAAC reaction (denoted with A), the product of one-pot Sonogashira – CuAAC reaction (denoted with B).

Although the reaction presented above demonstrated the ability of **PAF-1** to act as catalyst for one-pot formation of a $Csp^2$-Csp bonds and a triazole ring, further optimisation of the reaction conditions (*e.g*., use of an excess of alkyne derivative, use a mixture of toluene/methanol as solvent, argon atmosphere etc.) are required. in order to improve the reaction yields.

## Conclusions

In summary, within this chapter we discussed the synthesis, characterization and catalytic behavior of two porous aromatic frameworks (**PAF-1** and **PAF-2**) which showed the ability to incorporate palladium and copper species, from the co-catalysts used in their Sonogashira cross-coupling synthesis, within their frameworks. The utility of entrapped metal species as catalysts in various reactions was demonstrated by direct use of **PAF-1** and **PAF-2** as heterogeneous catalysts in Suzuki-Miyaura, Stille and Sonogashira cross-coupling reactions as well as in CuAAC *click* triazole synthesis and one-pot CuAAC – Sonogashira.

The results on Suzuki cross-coupling reactions showed that both materials present high catalytic activity using both boronic acids and pinacol boronic esters as coupling partners with different halides. As expected, the reaction yields were proved to be highly dependent on the electronic properties of the substituents at the para positions.

**PAF-1** also showed good catalytic properties in alkyne-azide cycloaddition reaction in both methanol or water as solvent. The conversions were quantitative when aliphatic alkynes were used and up to 73 % when aromatic alkyne was used as reaction partners.

Moreover, preliminary results have shown the potential of **PAF-1** as a heterogeneous catalyst in Stille cross-coupling reactions.

In addition, we proved that the palladium and copper species entrapped within the framework can be simultaneously employed to efficiently promote Sonogashira cross-coupling reaction with both aliphatic or aromatic alkyne in either toluene or water as solvent and triethylamine as base.

Finally, using an iodo and azido functionalized substrate, we demonstrated that our catalyst can be also used, although with modest conversions, for one pot CuAAC - Sonogashira cross-coupling reactions.

## GENERAL CONCLUSIONS

Investigation of the three isomers of IDT system showed a significant change in optoelectronic properties depending on the junction of the thiophene rings to the central benzene unit.

The investigations made on compound *1*, *2* and *3* revealed the most suitable HOMO/ LUMO values for organic solar cells when the thiophene units are joined through $\alpha$-position to the phenyl ring (**IDT- 1**) and they are less appropriate in case of $\beta$-position linking (**IDT-2** and **IDT-3**).

The examination of new symmetric and nonsymmetric compounds based on fused ring system (**IDT-1**) with various end-capping units in bulk heterojunction organic solar cells showed an acceptor behavior for five of them (compounds *1*, *18-21*) and a donor behavior for one compound (*22*).

We have also obtained five new compounds, of D-A type (*32-36*) acting as a single material for organic solar cells, being the smallest molecules with this specific characteristic known in the literature. Remarkable power conversion efficiency (0.86 - 0.88%) and short-circuit current (3.28 - 3.50 mAcm$^{-2}$) were obtained.

Two new porous aromatic frameworks, namely *PAF-1* and *PAF-2*, which showed the ability to incorporate palladium and copper species within their frameworks have been synthesized by Sonogashira cross-coupling reaction, characterized and used as catalysts for some cross-coupling reactions like Suzuki-Miyaura cross-coupling reaction, Stille ross-coupling reaction, alkyne-azide cycloaddition reaction and Sonogashira cross-coupling reactions.

## List of publications

1. *Structure-properties of small donor-acceptor molecules for homojunction single-material organic solar cells*

**Natalia Terenti**, Gavril-Ionel Giurgi, Andreea Petronela Crişan, Cătălin Anghel, Alexandra Bogdan, Alexandra Pop, Ioan Stroia, Anamaria Terec, Lorant Szolga, Ion Grosu, Jean Roncali

*Journal of Materials Chemistry C, 2022, 10, 5716-5726.*

2. *Effect of the Terminal Acceptor Unit on the Performance of Non-Fullerene Indacenodithiophene Acceptors in Organic Solar Cells*

**Natalia Terenti**, Gavril-Ionel Giurgi, Lorant Szolga, Ioan Stroia, Anamaria Terec, Ion Grosu and Andreea Petronela Crişan

*Molecules 2022, 27, 1229-1244.*

3. *Sonogashira Synthesis of New Porous Aromatic Framework Entrapped Palladium Nanoparticles as Heterogeneous Catalysts for Suzuki−Miyaura Cross-Coupling*

Lidia Căta, **Natalia Terenti,** Cristina Cociug, Niculina Daniela Hădade, Ion Grosu, Cristina Bucur, Bogdan Cojocaru, Vasile I. Parvulescu, Michal Mazur and Jiří Čejka

*ACS Applied Materials & Interfaces, 2022, 14, 10428–10437.*

4. *Effect of the mode of fixation of the thienyl rings on the electronic properties of electron acceptors based on indacenodithiophene (IDT)*

**Natalia Terenti**, Andreea Petronela Crişan, Siriporn Jungsuttiwong, Niculina Daniela Hadade, Alexandra Pop, Ion Grosu, Jean Roncali

*Dyes and Pigments, 2021, 187, 109116-109125.*

5. *Procedeu pentru obtinerea de celule solare organice stabile de tipul ITO/ZnO/Donor + Acceptor/MoO$_3$/Al folosind un donor de tip indacenoditiofenic si acceptori fulerenici (PC$_{61}$BM)*

**Natalia Terenti**, Gavril-Ionel Giurgi, Lorant Szolga, Ion Grosu

*Brevet de inventie  depus la OSIM fiind inregistrat cu nr. A/00195 din 10.04.2020*